Article

Structure of the Charge Separated State in the Photosynthetic Reaction Centers of *Rhodobacter sphaeroides* by Quantum Beat Oscillations and High-Field Electron Paramagnetic Resonance: Evidence for Light-Induced Reorientation

Ulrich Heinen, Lisa M. Utschig, Oleg G. Poluektov, Gerhard Link, Ernst Ohmes, and Gerd Kothe

J. Am. Chem. Soc., **2007**, 129 (51), 15935-15946 • DOI: 10.1021/ja075065h

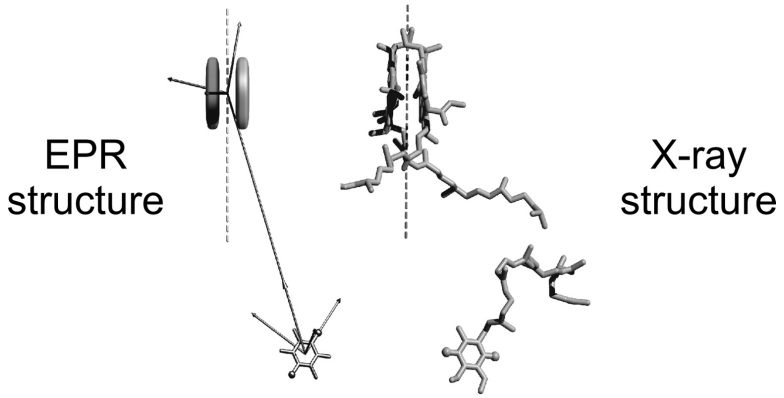

J|A|C|S
ARTICLES
Published on Web 12/05/2007

Structure of the Charge Separated State $P^+_{865}Q^-_A$ in the Photosynthetic Reaction Centers of *Rhodobacter sphaeroides* by Quantum Beat Oscillations and High-Field Electron Paramagnetic Resonance: Evidence for Light-Induced Q^-_A Reorientation

Ulrich Heinen,[†,§] Lisa M. Utschig,[‡] Oleg G. Poluektov,[‡] Gerhard Link,[†] Ernst Ohmes,[†] and Gerd Kothe*[,†]

Contribution from the Department of Physical Chemistry, University of Freiburg, Albertstrasse 21, D-79104 Freiburg, Germany, and Chemistry Division, Argonne National Laboratory, 7900 South Cass Avenue, Argonne, Illinois 60439

Received July 9, 2007; E-mail: gerd.kothe@physchem.uni-freiburg.de

Abstract: The structure of the secondary radical pair, $P^+_{865}Q^-_A$, in fully deuterated and Zn-substituted reaction centers (RCs) of the purple bacterium *Rhodobacter sphaeroides* R-26 has been determined by high-time resolution and high-field electron paramagnetic resonance (EPR). A computer analysis of quantum beat oscillations, observed in a two-dimensional Q-band (34 GHz) EPR experiment, provides the orientation of the various magnetic tensors of $P^+_{865}Q^-_A$ with respect to a magnetic reference frame. The orientation of the *g*-tensor of P^+_{865} in an external reference system is adapted from a single-crystal W-band (95 GHz) EPR study [Klette, R.; Törring, J. T.; Plato, M.; Möbius, K.; Bönigk, B.; Lubitz, W. *J. Phys. Chem.* **1993**, *97*, 2015−2020]. Thus, we obtain the three-dimensional structure of the charge separated state $P^+_{865}Q^-_A$ on a nanosecond time scale after light-induced charge separation. Comparison with crystallographic data reveals that the position of the quinone is essentially the same as that in the X-ray structure. However, the head group of Q^-_A has undergone a 60° rotation in the ring plane relative to its orientation in the crystal structure. Analysis suggests that the two different Q_A conformations are functionally relevant states which control the electron-transfer kinetics from Q^-_A to the secondary quinone acceptor Q_B. It appears that the rate-limiting step of this reaction is a reorientation of Q^-_A in its binding pocket upon light-induced reduction. The new kinetic model accounts for striking observations by Kleinfeld et al. who reported that electron transfer from Q^-_A to Q_B proceeds in RCs cooled to cryogenic temperature under illumination but does not proceed in RCs cooled in the dark [Kleinfeld, D.; Okamura, M. Y.; Feher, G. *Biochemistry* **1984**, *23*, 5780−5786].

Introduction

The primary energy conversion steps of photosynthesis involve a series of light-induced electron-transfer reactions which occur in specific membrane-bound proteins, the so-called reaction centers (RCs). The arrangement of the cofactors in the RC of purple bacteria is well characterized by X-ray crystallography.[1−4] Generally, charge separation is initiated by photoexcitation of the primary donor, P_{865}, which consists of two closely positioned bacteriochlorophyll molecules.[5] In the RC of *Rhodobacter (Rb.) sphaeroides* an electron is transferred within 200 ps from the excited singlet state of P_{865} to the secondary acceptor, ubiquinone Q_A,[6−8] through the intervening bacteriopheophytin acceptor, Φ_A. The radical pair $P^+_{865}Q^-_A$ is the most readily detected intermediate observable by time-resolved electron paramagnetic resonance (EPR). At room temperature the electron is further transferred in about 100 μs to the tertiary acceptor, ubiquinone Q_B, which serves as a sequential two-electron acceptor and redox shuttle.[6−8] Thus, the electron-transfer reactions in the RC of *Rb. sphaeroides* can be written as

$$P_{865}\Phi_A Q_A Q_B \xrightarrow{h\nu} {}^1P^*_{865}\Phi_A Q_A Q_B \rightarrow P^+_{865}\Phi_A^- Q_A Q_B \rightarrow P^+_{865}\Phi_A Q_A^- Q_B \rightarrow P^+_{865}\Phi_A Q_A Q_B^- \quad (1)$$

In native RCs, the radical pair $P^+_{865}Q^-_A$ is created in a virtually pure singlet state, determined by the spin multiplicity

[†] University of Freiburg.
[‡] Argonne National Laboratory.
[§] Present address: Bruker Biospin MRI GmbH, Rudolf-Plank-Strasse 23, 76275 Ettlingen, Germany.

(1) Deisenhofer, J.; Epp, O.; Miki, K.; Huber, R.; Michel, H. *J. Mol. Biol.* **1984**, *180*, 385−398.
(2) Komiya, H.; Yeates, T.; Rees, D.; Allen, J.; Feher, G. *Proc. Natl. Acad. Sci. U.S.A.* **1988**, *85*, 9012−9016.
(3) Chang, C.-H.; El-Kabbani, O.; Tiede, D.; Norris, J. R.; Schiffer, M. *Biochemistry* **1991**, *30*, 5352−5360.
(4) Ermler, U.; Fritzsch, G.; Buchanan, S.; Michel, H. *Structure* **1994**, *2*, 925−936.
(5) Norris, J. R.; Uphaus, R. A.; Crespi, H. L.; Katz, J. J. *Proc. Natl. Acad. Sci. U.S.A.* **1971**, *68*, 625−628.
(6) Feher, G.; Okamura, M.; McElroy, J. *Biochim. Biophys. Acta* **1972**, *267*, 222−226.
(7) Okamura, M. Y.; Isaacson, R. A.; Feher, G. *Proc. Natl. Acad. Sci. U.S.A.* **1975**, *72*, 3491−3495.
(8) Okamura, M. Y.; Feher, G. In *Anoxygenic Photosynthetic Bacteria*; Blankenship, R. E., Madigan, M. T., Bauer, C. E., Eds.; Kluwer Academic Publishers: Dordrecht, 1994; pp 577−594.

of the excited bacteriochlorophyll donor $^1P^*_{865}$. Generally, such a singlet radical pair is formed with spin-correlated population of only one-half of the eigenstates.[9−11] This gives rise to high electron spin polarization. In addition, there are coherences between the eigenstates of the radical pair, which can manifest themselves as quantum beats in an EPR experiment with adequate time resolution.[12−19] The electron spin polarization of $P^+_{865}Q^-_A$ has been exploited in probing the geometry of the radicals in the pair.[20,21] Analysis of the time-resolved K- (24 GHz) and W-band (95 GHz) EPR spectra was achieved on the basis of the published X-ray structures.[20,21]

The light-induced electron transfer from Q^-_A to Q_B has been the subject of numerous investigations. Based on a detailed study of the reaction kinetics, it was concluded that this process is conformationally gated, i.e., that the rate-limiting step is a conformational change required before electron transfer.[22] This change was proposed to be a movement of Q_B as observed in a high-resolution X-ray study of single crystals of the *Rb. sphaeroides* RC protein frozen under illumination and in the dark.[23] The analysis revealed that Q_B in the light-excited (reduced) state is located approximately 5 Å from the Q_B position in the dark adapted (neutral) state and has undergone a 180° propeller twist of its head group.[23,24] However, recent Fourier transform infrared (FTIR) studies of RCs of *Rb. sphaeroides* do not indicate different bonding of neutral and reduced Q_B to the protein.[25] Rather, light-induced FTIR difference spectroscopy suggests a change of the bonding situation upon reduction only for Q_A.[26]

Evidently, the molecular details of the electron transfer from Q^-_A to Q_B are not yet fully understood. If the observed displacement of Q_B[23,24] is not related to this gated process, which other conformational changes could be relevant? Is Q_A involved in the gating mechanism as suggested by FTIR spectroscopy?[26] The objective of the present study is to obtain a unique structure of Q^-_A, and, thus, to shed light on the electron-transfer mechanism. To achieve this goal, we determine the geometry of $P^+_{865}Q^-_A$ using quantum beat oscillations of the spin-correlated radical pair.[27] This approach is more specific than X-ray crystallography of the RC protein, where due to radiation-induced photoelectrons[28] the reduction states of the quinones are not known. Thus, we expect that the structural data of the $P^+_{865}Q^-_A$ radical pair may help in clarifying the function of Q_A in the electron transfer from Q^-_A to Q_B.

We first present a time-resolved Q-band (34 GHz) EPR study of $P^+_{865}Q^-_A$ in fully deuterated and Zn-substituted RCs of *Rb. sphaeroides* R-26. The experiment is performed on dark adapted samples at low temperature where electron transfer from Q^-_A to Q_B is impaired. A computer analysis of the observed Q-band quantum oscillations provides the orientation of the various magnetic tensors of $P^+_{865}Q^-_A$ with respect to a magnetic reference frame. The obtained geometry is checked by simulation of the spin-polarized W-band EPR spectrum of $P^+_{865}Q^-_A$.

The orientation of the *g*-tensor of P^+_{865} in an external reference system is adapted from a previous W-band EPR study performed on single crystals of the RC protein.[29] A fourfold structural ambiguity, which is a general problem in these studies, has been eliminated by a combined analysis of the Q- and W-band EPR results. Thus, we obtain the three-dimensional structure of the radical pair intermediate $P^+_{865}Q^-_A$ on a nanosecond time scale after light-induced charge separation.

The geometry of the charge separated state, $P^+_{865}Q^-_A$, describes the position and orientation of the reduced acceptor, Q^-_A, in the photosynthetic RC. A detailed comparison reveals that the orientation of Q^-_A in the radical pair is significantly different from that of Q_A in the X-ray structure, suggesting a conformational change of Q^-_A in connection with the electron transfer to Q_B. The results are rationalized in terms of a new kinetic model for this process.

Theoretical Background

In this section we briefly summarize a quantum-mechanical model used in the analysis of transient Q-band EPR experiments performed on the spin-correlated radical pair $P^+_{865}Q^-_A$ in fully deuterated RCs. Particular emphasis is given to quantum beat oscillations detectable at early times after laser pulse excitation.[12−19] The quantum beats are highly sensitive probes for the geometry of the charge separated state.[27]

In a frame rotating with the microwave frequency ω around the static magnetic field $\mathbf{B}_0$, the total spin Hamiltonian, $H(\Omega)$, of the radical pair can be written as

$$H(\Omega) = \mu_B B_0(g_1^{zz}(\Omega)\, S_1^z + g_2^{zz}(\Omega)\, S_2^z) - \hbar\omega(S_1^z + S_2^z) +$$
$$+ 2(D^{zz}(\Omega) - J_{ex})S_1^z S_2^z - \left(\frac{1}{2} D^{zz}(\Omega) + J_{ex}\right)(S_1^- S_2^+ + S_1^+ S_2^-) +$$
$$+ \sum_k a_{1k} S_1^z I_{1k}^z + \sum_l a_{2l} S_2^z I_{2l}^z + \frac{1}{2}(g_1 + g_2)\mu_B B_1(S_1^x + S_2^x) \quad (2)$$

where μ_B, B_0, $g_i^{zz}(\Omega)$, S_i^z, $D^{zz}(\Omega)$, J_{ex}, $S_i^-(S_i^+)$, a_{ij}, I_{ij}^z, g_i, B_1, and S_i^x are the Bohr magneton, the strength of the static magnetic field, the *zz* component of the *g*-tensor $\mathbf{g}_i$, the *z* component of the electron spin operator $\mathbf{S}_i$, the *zz* component of the dipolar

(9) Thurnauer, M. C.; Norris, J. R. *Chem. Phys. Lett.* **1980**, *76*, 557−561.
(10) Closs, G. L.; Forbes, M. D. E.; Norris, J. R. *J. Phys. Chem.* **1987**, *91*, 3592−3599.
(11) Buckley, C. D.; Hunter, D. A.; Hore, P. J.; McLauchlan, K. A. *Chem. Phys. Lett.* **1987**, *135*, 307−312.
(12) Salikhov, K. M.; Bock, C. H.; Stehlik, D. *J. Appl. Magn. Reson*. **1990**, *1*, 195−211.
(13) Bittl, R.; Kothe, G. *Chem. Phys. Lett*. **1991**, *177*, 547−553.
(14) Kothe, G.; Weber, S.; Bittl, R.; Ohmes, E.; Thurnauer, M. C.; Norris, J. R. *Chem. Phys. Lett*. **1991**, *186*, 474−480.
(15) Zwanenburg, G.; Hore, P. J. *Chem. Phys. Lett.* **1993**, *203*, 65−74.
(16) Kothe, G.; Weber, S.; Ohmes, E.; Thurnauer, M. C.; Norris, J. R. *J. Phys. Chem.* **1994**, *98*, 2706−2712.
(17) Kothe, G.; Weber, S.; Ohmes, E.; Thurnauer, M. C.; Norris, J. R. *J. Am. Chem. Soc*. **1994**, *116*, 7729−7734.
(18) Bittl, R.; van der Est, A.; Kamlowski, A.; Lubitz, W.; Stehlik, D. *Chem. Phys. Lett*. **1994**, *226*, 349−358.
(19) Kothe, G.; Bechtold, M.; Link, G.; Ohmes, E.; Weidner, J.-U. *Chem. Phys. Lett.* **1998**, *283*, 51−60.
(20) van der Est, A.; Bittl, R.; Abresch, E. C.; Lubitz, W.; Stehlik, D. *Chem. Phys. Lett.* **1993**, *212*, 561−568.
(21) Prisner, T. F.; van der Est, A.; Bittl, R.; Lubitz, W.; Stehlik, D.; Möbius, K. *Chem. Phys.* **1995**, *194*, 361−370.
(22) Graige, M. S.; Feher, G.; Okamura, M. Y. *Proc. Natl. Acad. Sci. U.S.A.* **1998**, *95*, 11679−11684.
(23) Stowell, M. H. B.; McPhillips, T. M.; Rees, D. C.; Soltis, S. M.; Abresch, E.; Feher, G. *Science* **1997**, *276*, 812−816.
(24) Fritzsch, G.; Koepke, J.; Diem, R.; Kuglstatter, A.; Baciou, L. *Acta Crystallogr*. **2002**, *D58*, 1660−1663.
(25) Breton, J.; Boullais, C.; Mioskowski, C.; Sebban, D.; Baciou, L.; Nabedryk, E. *Biochemistry* **2002**, *41*, 12921−12927.
(26) Breton, J.; Burie, J.-R.; Berthomieu, C.; Berger, G.; Nabedryk, G. *Biochemistry* **1994**, *33*, 4953−4965.
(27) Link, G.; Berthold, T.; Bechtold, M.; Weidner, J.-U.; Ohmes, E.; Tang, J.; Poluektov, O.; Utschig, L.; Schlesselman, S. L.; Thurnauer, M. C.; Kothe, G. *J. Am. Chem. Soc.* **2001**, *123*, 4211−4222.
(28) Weik, M.; Ravelli, R. B. G.; Kryger, G.; McSweeney, S.; Raves, M. L.; Havel, M.; Gros, P.; Silman, I.; Kroon, J.; Sussman, J. L. *Proc. Natl. Acad. Sci. U.S.A.* **2000**, *97*, 623−628.
(29) Klette, R.; Törring, J. T.; Plato, M.; Möbius, K.; Bönigk, B.; Lubitz, W. *J. Phys. Chem.* **1993**, *97*, 2015−2020.

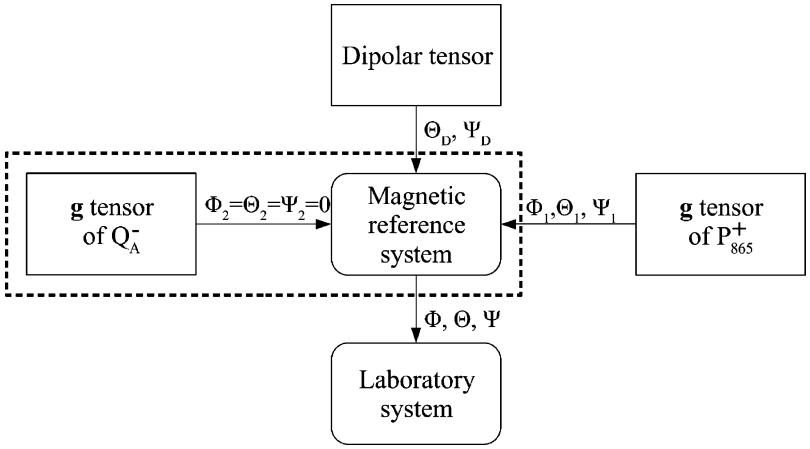

Figure 1. Notation for magnetic tensor systems and Euler transformations used in the EPR model. For convenience, the magnetic reference system is chosen parallel to the *g*-tensor of Q_A^-. P_{865} = primary electron donor. Q_A = secondary electron acceptor.

coupling tensor $\mathbf{D}(\Omega)$, the strength of the isotropic exchange interaction,[30] the lowering (raising) operator of electron *i*, the isotropic hyperfine coupling between nucleus *j* and radical *i*,[31] the *z* component of the nuclear spin operator $\mathbf{I}_{ij}$, the isotropic *g*-factor of radical *i*, the strength of the microwave field, and the *x* component of the electron spin operator $\mathbf{S}_i$, respectively. Note that nonsecular terms of the electron spin−spin interactions (see eq 2, fourth term) are explicitely considered in the analysis. These terms are essential for the modeling of quantum oscillations and thus provide the basis for the structure determination.

The orientation dependence of the magnetic tensor elements $g_i^{zz}(\Omega)$ and $D^{zz}(\Omega)$ can be evaluated by a twofold transformation from the principal axis system $\mathbf{X}_i$, $\mathbf{Y}_i$, $\mathbf{Z}_i$. In the first step we transform to a common reference system **X**, **Y**, **Z**, using the Euler angles,[32] $\Omega_i = (\Phi_i,\Theta_i,\Psi_i)$ (see Figure 1). For convenience, this reference system is chosen parallel to the principal axis system of the *g*-tensor of Q_A^-. In the second step we transform by the Euler angles[32] $\Omega = (\Phi,\Theta,\Psi)$ into the laboratory frame **x**, **y**, **z**, with $\mathbf{B}_0$ along the *z*-axis. A random distribution of the radical pair with respect to the laboratory frame is considered by averaging over the Euler angles Φ, Θ, and Ψ (see Figure 1).

The crucial point is the specification of the initial condition of $P_{865}^+Q_A^-$ at the instant of the laser pulse. In native photosynthetic RCs of *Rb. sphaeroides*, the lifetime of the primary radical pair, $P_{865}^+Q_A^-$, is short, i.e., approximately 200 ps. Thus, even the secondary radical pair is generated in a virtually pure singlet state, determined by the spin multiplicity of the excited primary donor. Generally, such a singlet radical pair is formed with spin-correlated population of only one-half of the eigenstates[9−11] and with zero quantum electron[12−19] and single quantum nuclear coherences[19] between these states. Analysis reveals that in Q- and W-band studies only zero quantum electron coherences can be observed.[19]

In the absence of a microwave field, the eigenstate populations are constant in time, while the *zero quantum electron coherences* oscillate at distinct frequencies[16,17,27]

$$\omega_{ZQ} = (1/\hbar)\left\{\left[\frac{2}{3}D^{zz}(\Omega) - 2J_{ex}\right]^2 + \right.$$
$$\left. + [(g_1^{zz}(\Omega) - g_2^{zz}(\Omega))\mu_B B_0 + \sum_k a_{1k} M_{1k}^i - \sum_l a_{2l} M_{2l}^j]^2\right\}^{1/2} \quad (3)$$
$$M_{1k}^i = I_{1k}, I_{1k} - 1, ..., -I_{1k}$$
$$M_{2l}^j = I_{2l}, I_{2l} - 1, ..., -I_{2l}$$

given by the energy separation of the corresponding eigenstates. Inspection of eq 3 reveals that ω_{ZQ} is determined by the spin−spin interactions in the radical pair and the difference in the Zeeman and hyperfine interactions of the constituent radicals. For $P_{865}^+Q_A^-$, the Zeeman term provides the largest contribution in Q-band EPR experiments.

The weak microwave field B_1, commonly employed in transient EPR, allows for only a small range of orientations to meet the resonance condition. As a result, the amplitude and frequency of the quantum oscillations vary significantly with B_0 across the powder spectrum. This pronounced variation can be used to evaluate the geometry of the charge separated state $P_{865}^+Q_A^-$ in the photosynthetic membrane. A computer analysis of the two-dimensional Q-band experiment provides the orientation of the various magnetic tensors with respect to a common reference frame. Thus, by studying the short-time spin dynamics, all five Euler angles characterizing the radical pair geometry are obtained.

As noted above, the Q-band experiments are performed using fully deuterated samples. Deuteration provides the greatly enhanced signal-to-noise ratio necessary for a successful detection of quantum oscillations. Furthermore, it slows down the rapid decay of the zero quantum electron precessions due to the difference in hyperfine interactions of the radical ions (see eq 3, last term). Finally, it allows for an improved orientation selection of the quantum beats in the two-dimensional Q-band experiment.

Materials and Methods

Sample Preparation. Deuterated RCs were isolated as previously described[33] from whole cells of the photosynthetic bacterium *Rb. sphaeroides* R-26 which were grown in D_2O (99.7%) on deuterated

(30) The sign of the exchange interaction parameter, J_{ex}, has been chosen to common practice.
(31) Reitz, D. C.; Weissman, S. I. *J. Chem. Phys.* **1960**, *33*, 700−704.
(32) Edmonds, A. R. *Angular Momentum in Quantum Mechanics*; Princeton University Press: Princeton, 1974; pp 6−8.
(33) Utschig, L. M.; Greenfield, S. R.; Tang, J.; Laible, P. D.; Thurnauer, M. C. *Biochemistry* **1997**, *36*, 8548−8558.

substrates.[34] The nonheme Fe^{2+} was removed from the RCs and replaced by Zn^{2+} by chaotropic treatment using the procedure of Utschig et al.[33] The electron-transfer rate from the intermediate acceptor Φ_A^- to the secondary acceptor Q_A was measured to be $(200\ ps)^{-1}$ for the Fe-removed/Zn-replaced samples used in the EPR experiments.[33] The RC samples were handled in the dark and stored at −70 °C.

Q-Band EPR Measurements. The time-resolved Q-band EPR experiments were carried out using a transient Q-band bridge (Bruker ER050QGT) in combination with a Bruker ESP300E console. Homemade software was used to set the magnetic field under the control of an NMR teslameter (Bruker ER035M). Drifts of the microwave frequency were compensated by a digital feedback loop. The magnetic field was calibrated against Li:LiF (Institute of Crystallography, Moscow), which is a good standard for low temperature measurements.[35] Irradiation of the sample was performed in a cylindrical cavity with a loaded Q of approximately 700. This corresponds to a bandwidth of 50 MHz. A frequency counter (Hewlett-Packard HP5352B) was used to monitor the microwave frequency in the Q-band range.

For optical excitation the frequency-doubled output of a Nd:YAG laser (Spectra Physics Quanta Ray GCR190-10) with a wavelength of 532 nm and a pulse width of 2.5 ns was used. The laser intensity was attenuated to 2−2.5 mJ/pulse, as measured after a quartz depolarizer located in the laser beam. The repetition rate of the laser was 10 Hz. A transient recorder (LeCroy 9354A) was used to digitize the signal with a time resolution of 2 ns at 11 bit precision. Typically, 400 to 600 transients were accumulated to improve the signal/noise ratio. A weak laser-induced cavity signal was eliminated by substracting transients accumulated at off-resonance conditions.

W-Band EPR Measurements. The high-field experiments were carried out on a Bruker ELEXSYS E680X W-band EPR spectrometer equipped with a TE_{011} cylindrical cavity and high bandwidth mixer detection. The field of the superconducting magnet was calibrated using Li:LiF (Institute of Crystallography, Moscow) as a standard.[35] Optical excitation of the sample was performed with 2.5 ns pulses from a Q-switched, frequency-doubled Nd:YAG laser (Spectra Physics Quanta Ray GCR130-15). The laser output was depolarized and attenuated to approximately 1 mJ/pulse. Excitation of the sample in the resonator was achieved using a fiber optic light path through the sample rod (silica optical fiber, 400 μm core diameter, Fiberguide Industries), as described previously.[36] The time-resolved EPR signal was recorded and averaged with a LeCroy 9354A digital oscilloscope. Typically, 500 transients were accumulated to improve the signal/noise ratio. Magneto-orientation effects[37] were not observed.

Computations. A Fortran program package,[38] based on the theoretical approach outlined in the preceding section, was used to analyze the time-resolved EPR experiments. The programs calculate EPR time profiles and transient spectra of spin-correlated radical pairs with a spatially fixed geometry. The structural parameters were evaluated using a nonlinear least-squares fit procedure based on the Levenberg−Marquardt algorithm.[39] All computations were performed on a SGI Origin 2000 computer. Parallel execution was utilized for the powder averaging procedure.

A set of 3500−4900 calculated data points covering the full spectral range and a time interval of 120 ns was simultaneously fitted to the experimental data set by varying the geometry parameters. The fit was repeated multiple times with different starting values covering the whole parameter space. The same global minimum values were found in about 30% of all runs.

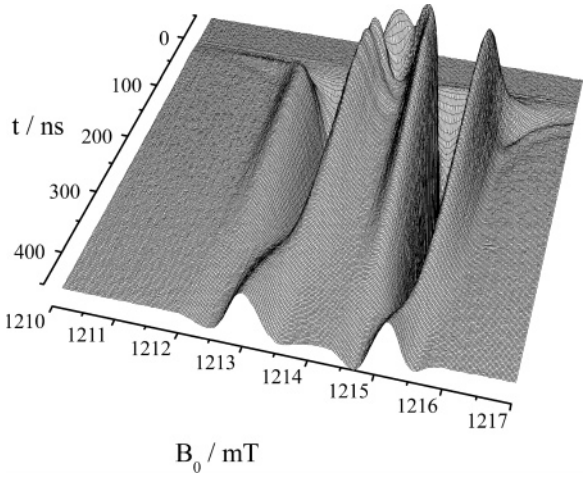

Figure 2. Two-dimensional Q-band data set of the light-induced radical pair $P_{865}^+Q_A^-$ in deuterated and Zn-substituted reaction centers of *Rhodobacter sphaeroides* R-26 frozen in the dark. Positive signals indicate absorptive and negative emissive spin polarization. Microwave frequency, $\omega/2\pi = 34.066$ GHz. Microwave field, $B_1 = 0.04$ mT. Temperature, $T = 70$ K. Quantum beat oscillations are clearly visible in the center and in the wings of the data set.

Results

Strategy of Structure Determination. Our strategy to obtain the structure of $P_{865}^+Q_A^-$ involves a high-time resolution Q-band EPR study of $P_{865}^+Q_A^-$ using a fully deuterated sample. Analysis of the anisotropic quantum oscillations provides the orientation of the various magnetic tensors of $P_{865}^+Q_A^-$ with respect to a magnetic reference frame. The obtained geometry is checked by simulation of the spin-polarized W-band EPR spectrum of $P_{865}^+Q_A^-$. The orientation of the *g*-tensor of P_{865}^+ in an external reference system was adapted from a previous W-band EPR study performed on single crystals of the RC protein.[29] Thus, we obtain the three-dimensional structure of the radical pair intermediate $P_{865}^+Q_A^-$ on a nanosecond time scale after light-induced charge separation.

Mutual Orientation of the Magnetic Tensors. Evaluation of the magnetic tensor orientations is based on transient nutation EPR experiments performed at Q-band frequencies. In these experiments, the sample is irradiated with a short laser pulse and the time evolution of the transverse magnetization is detected in the presence of a weak microwave magnetic field. Generally, a complete data set consists of transient signals taken at equidistant field points covering the total spectral width. This yields a two-dimensional variation of the signal intensity with respect to both the magnetic field and the time axis.

Such a complete data set for $P_{865}^+Q_A^-$, measured at Q-band frequencies ($\omega/2\pi = 34.066$ GHz), is shown in Figure 2. The data set refers to fully deuterated and Zn-substituted RCs of *Rb. sphaeroides* R-26, a microwave field of $B_1 = 0.04$ mT and $T = 70$ K. Positive signal intensities indicate absorptive (a) and negative emissive (e) spin polarization. Transient spectra can be extracted from this plot at any fixed time after the laser pulse as slices parallel to the magnetic field axis. Likewise, the time evolution of the transverse magnetization may be obtained for any given field as a slice along the time axis. Note the pronounced modulations in the transverse magnetization. These

(34) Crespi, H. L. *Methods Enzymol.* **1982**, *88*, 3−5.
(35) Cherkasov, F. G.; Denisenko, G. A.; Vitol, A. Ya.; L'vov, S. G. In *Proceedings of the XXVIIth Congress Ampère on Magnetic Resonance and Related Phenomena*; Salikhov, K. M., Ed.; Zavoisky Physical-Technical Institute: Kazan, 1994; Vol. 1, pp 416−417.
(36) Hofbauer, W.; Bittl, R. *Bruker Report* **1998**, *145*, 38−39.
(37) Heinen, U.; Poluektov, O. G.; Stavitski, E.; Berthold, T.; Ohmes, E.; Schlesselman, S. L.; Golecki, J. R.; Moro, G. J.; Levanon, H.; Thurnauer, M. C.; Kothe, G. *J. Phys. Chem. B* **2004**, *108*, 9498−9504.
(38) Laukenmann, K. Ph.D. Thesis, University of Freiburg, 1999.
(39) Marquardt, D. W. *J. Soc. Indust. Appl. Math.* **1963**, *11*, 431−441.

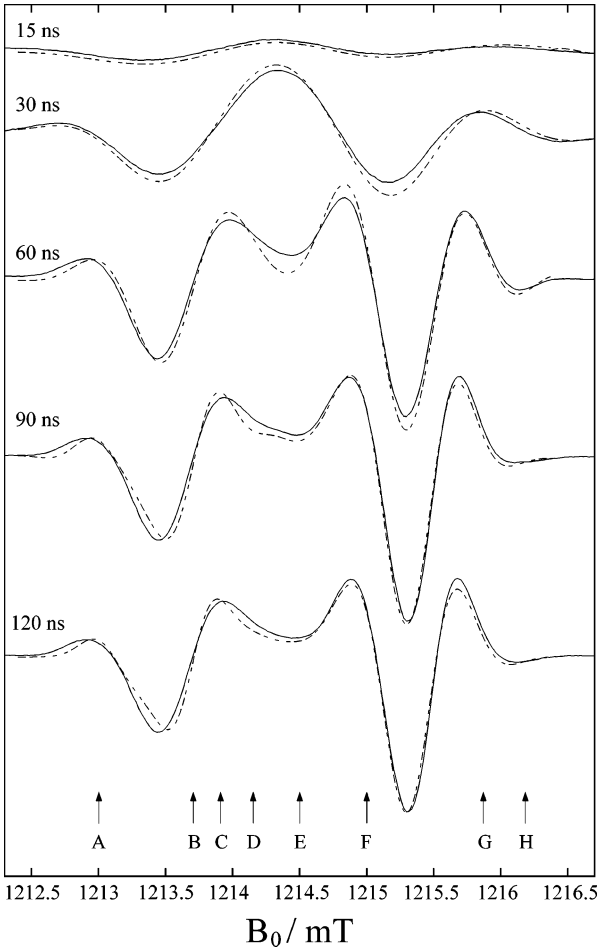

Figure 3. Transient Q-band EPR spectra of the light-induced radical pair $P_{865}^+Q_A^-$ in reaction centers of purple bacteria at various times after the laser pulse. Positive signals indicate absorptive and negative emissive spin polarization. Microwave frequency, $\omega/2\pi = 34.066$ GHz. Microwave field, $B_1 = 0.04$ mT. Full lines: Experimental spectra from deuterated and Zn-substituted reaction centers of *Rhodobacter sphaeroides* R-26 frozen in the dark. Temperature, $T = 70$ K. Dashed lines: Calculated spectra using the parameters given in Table 1. Various field positions are marked from A to H. The time evolution of the transverse magnetization at these field positions is shown in Figure 4.

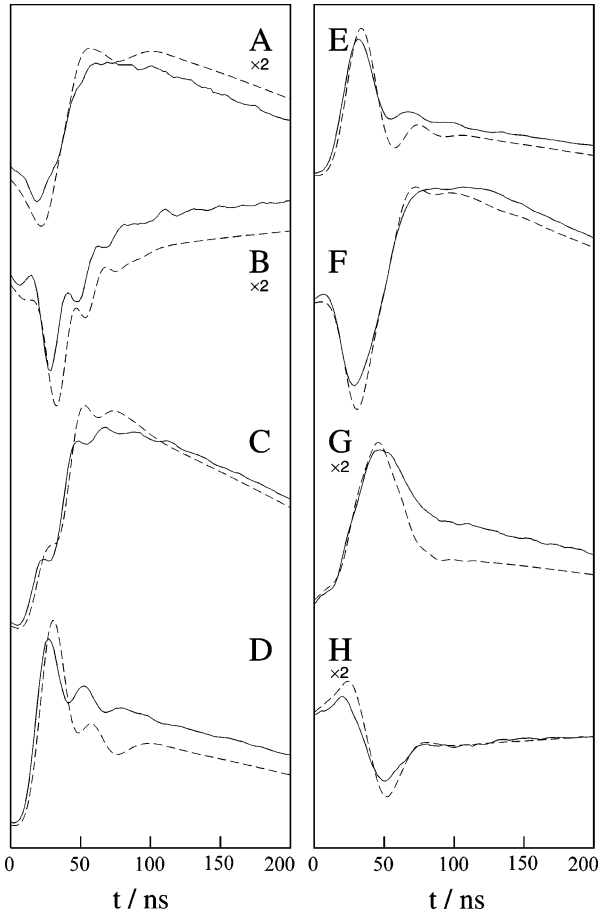

Figure 4. Time evolution of the transverse Q-band magnetization of the light-induced radical pair $P_{865}^+Q_A^-$ in reaction centers of purple bacteria immediately after the laser pulse. The transients refer to eight different static magnetic fields (positions A-H, Figure 3). Positive and negative signals indicate absorptive and emissive polarizations, respectively. Microwave frequency, $\omega/2\pi = 34.066$ GHz. Microwave field, $B_1 = 0.04$ mT. Full lines: Experimental time profiles from deuterated and Zn-substituted reaction centers of *Rhodobacter sphaeroides* R-26 frozen in the dark. Temperature, $T = 70$ K. Dashed lines: Calculated time profiles using the parameters given in Table 1.

consist of fast quantum beat oscillations which disappear shortly after the laser flash and slow persisting Torrey oscillations[40] with frequencies of a few MHz.

Typical Q-band EPR spectra, extracted at five different times after the laser pulse, are shown in Figure 3 (solid lines). Evidently, the early spectrum is much broader than the later ones. Moreover, the polarization changes from a simple e/a/e/a pattern at early times to a characteristic a/e/a/a/e/a pattern at later times. It can be assigned to the secondary radical pair $P_{865}^+Q_A^-$ of the electron-transfer chain. Figure 4 depicts the short time behavior of the transverse magnetization (solid lines) measured at eight selected field positions (A−H, Figure 3). Evidently, there are fast initial oscillations which disappear 100 ns after the laser pulse. Basically, these oscillations represent quantum beats associated with the spin-correlated generation of the radical pair.[12−19] Note that the amplitude and frequency of the quantum beats vary significantly across the powder spectrum. This pronounced variation can be used to evaluate the mutual orientation of the magnetic tensors in $P_{865}^+Q_A^-$.

The fixed magnetic parameters, underlying the analysis of the two-dimensional Q-band experiment, are summarized in Table 1 (columns 1−4). The *g*-tensor components of P_{865}^+ and Q_A^- have been determined by a number of groups under different experimental conditions and thus vary moderately.[29,41−44] The quoted values were adapted from a W-band EPR study of the two radical ions in frozen solution under identical conditions.[41] The listed spin−spin coupling parameters are based on electron spin echo envelope modulation (ESEEM) studies of $P_{865}^+Q_A^-$.[45]

The parameters of the hyperfine interactions in the radical pair have been determined by ^{1}H electron nuclear double resonance (ENDOR) and ^{15}N ESEEM studies of the corre-

(40) Torrey, H. C. *Phys. Rev.* **1949**, *76*, 1059−1072.

(41) Burghaus, O.; Plato, M.; Rohrer, M.; Möbius, K.; MacMillan, F.; Lubitz, W. *J. Phys. Chem.* **1993**, *97*, 7639−7647.
(42) Wang, W.; Belford, R. L.; Clarkson, R. B.; Davis, P. H.; Forrer, J.; Nilges, M. J.; Tinken, M. D.; Walczak, T.; Thurnauer, M. C.; Norris, J. R.; Morris, A. L.; Zhang, Y. *Appl. Magn. Reson.* **1994**, *6*, 195−215.
(43) Isaacson, R. A.; Lendzian, F.; Abresch, E. C.; Lubitz, W.; Feher, G. *Biophys. J.* **1995**, *69*, 311−322.
(44) Bratt, P.; Ringus, E.; Hassan, A.; Tol, H. V.; Maniero, A.-L.; Brunel, L.-C.; Rohrer, M.; Bubenzer-Hange, C.; Scheer, H.; Angerhofer, A. *J. Phys. Chem. B* **1999**, *103*, 10973−10977.
(45) Bittl, R.; Zech, S. *J. Phys. Chem. B* **1997**, *101*, 1429−1436.

Table 1. Magnetic and Structural Parameters Used in the Analysis of Transient Q- and W-Band EPR Experiments of the Light-Induced Radical Pair, $P_{865}^{+}Q_A^{-}$, in Deuterated and Zn-Substituted Reaction Centers of *Rb. sphaeroides* R-26

g-tensor components[a] P_{865}^{+} Q_A^{-}	spin-spin coupling[b]	hyperfine interactions[c] P_{865}^{+} Q_A^{-}	line broadening[d]	g_1-tensor orientation[e]	dipolar tensor orientation[e]
g_1^X 2.00330 g_2^X 2.00660	D, -0.125 mT	5 ^{14}N nuclei; 4 ^{2}H nuclei	ΔB_0 = 0.29 mT	Φ_1, 26°	Φ_D, arbitr.
g_1^Y 2.00250 g_2^Y 2.00548	E, 0 mT	a_N 0.0838 mT; a_D 0.0411 mT		Θ_1, 114°	Θ_D, 67°
g_1^Z 2.00210 g_2^Z 2.00220	J_{ex}, 0 mT			Ψ_1, 73°	Ψ_D, 122°

[a] Data from a W-band EPR study.[41] Note that the literature value of g_2^Y has been slightly increased for this study in accordance with other investigations of this *g*-tensor. [b]Parameters from an ESEEM study of $P_{865}^{+}Q_A^{-}$.[45] [c]The hyperfine interactions in $P_{865}^{+}Q_A^{-}$ were approximated by considering five equivalent ^{14}N nuclei in P_{865}^{+} and four equivalent ^{2}H nuclei in Q_A^{-}.[46−50] This corresponds to second moments of $\langle B_0^2\rangle = 23.4 \times 10^{-3}$ mT^2 and $\langle B_0^2\rangle = 4.5 \times 10^{-3}$ mT^2. [d]Inhomogeneous broadening is considered by convolution with a Gaussian of line width $\Delta B_0 = 0.29$ mT. [e]Evaluated in the present study from a two-dimensional Q-band experiment using the anisotropy of quantum beat oscillations. The Euler angles (see Figure 1) relate the principal axis system of the respective magnetic tensor (*g*-tensor of P_{865}^{+}, dipolar tensor) and the magnetic reference system (*g*-tensor of Q_A^{-}).

sponding radical ions.[46−50] For the analysis of the Q-band EPR experiment, the hyperfine interactions in $P_{865}^{+}Q_A^{-}$ were *approximated* by considering five equivalent ^{14}N nuclei (a_N = 0.0838 mT) in P_{865}^{+} and four equivalent ^{2}H nuclei ($a_D = 0.0411$ mT) in Q_A^{-} (see Table 1, columns 4 and 5). This corresponds to second moments of $\langle B_0^2\rangle = 23.4 \times 10^{-3}$ mT^2 and $\langle B_0^2\rangle = 4.5 \times 10^{-3}$ mT^2, in agreement with the published hyperfine parameters for P_{865}^{+} and Q_A^{-}. Model calculations have shown that the use of equivalent ^{14}N and ^{2}H nuclei is a good approximation which considerably reduces the computational effort. Inhomogeneous broadening was considered by convolution with a Gaussian of line width $\Delta B_0 = 0.29$ mT.

The orientation of the magnetic tensors of $P_{865}^{+}Q_A^{-}$ (*g*-tensors, dipolar tensor) with respect to a magnetic reference system (*g*-tensor of Q_A^{-}) can be described by the five Euler angles Φ_1, Θ_1, Ψ_1, Θ_D, and Ψ_D (see Figure 1). Values for these angles were obtained from a computer fit of the two-dimensional Q-band experiment (see Figure 2) using the pronounced variation of the quantum beats across the powder spectrum. Notably, the full spectral width of 3.4 mT and a time range of 120 ns were considered. Thus, 58 calculated time profiles involving 3500 data points were simultaneously fitted to the experimental profiles by varying the parameters of the tensor orientations. In the calculations, the limited resonator bandwidth of 50 MHz was taken into account by using a Gaussian response function. Finally, spin relaxation was considered by multiplying each time profile by an exponential decay curve, characterized by the transverse relaxation time T_2. The values of T_2 vary slightly across the powder spectrum, exhibiting $T_2 \approx 1$ μs at the high-field emissive maximum.

The fit was repeated multiple times with different starting values covering the whole parameter space. The same global minimum values were found in about 30% of all runs. In the remaining fits local side minima were reached. The nearest side minimum with only a slightly bigger error sum was eliminated since it leads to an unreasonably large shift of Q_A^{-} of more than 7 Å relative to its position in the X-ray structure. In Figures 3 and 4 we compare experimental line shapes and time profiles (solid lines) with the best fit simulation (dashed lines) based on the parameter values (see Table 1, columns 7 and 8)

$$\Phi_1 = 26° \pm 4°,\ \Theta_1 = 114° \pm 8°,\ \Psi_1 = 73° \pm 5°$$

$$\Theta_D = 67° \pm 3°,\ \Psi_D = 122° \pm 2°$$

Generally, the agreement achieved is good. The cited errors are systematic errors, evaluated as described below.

It should be noted that the given geometry represents a selected set of 32 magnetically equivalent tensor orientations obtained from the fit of the two-dimensional Q-band EPR experiment. This structural ambiguity is a general problem in the analysis of magnetic resonance experiments since these techniques can principally not distinguish between a positive and a negative magnetic axis orientation. In fact, the two *g*-tensors exhibit D_{2h} symmetry and are therefore invariant under 180° rotations about their principal axes.[51] The axially symmetric dipolar tensor transforms according to the point group $D_{\infty h}$. Consequently, it is invariant under 180° rotation about any axis perpendicular to the symmetry axis.[51] The resulting ambiguity can be eliminated by a critical evaluation of the radical pair structures calculated from the various Q-band geometries and the known orientation of the *g*-tensor of P_{865}^{+}.[29] The crucial parameter is the position of Q_A^{-} in the photosynthetic membrane (see next section).

To verify the result of the fit, a second Q-band EPR data set has been analyzed. The experiment was performed at a different

(46) Käss, H.; Rautter, J.; Bönigk, B.; Höfer, P.; Lubitz, W. *J. Phys. Chem.* **1995**, *99*, 436−448.
(47) Isaacson, A. R.; Abresch, E.; Feher, G.; Lubitz, W.; Williams, J.; Allen, J. P. *Biophys. J.* **1995**, *68*, A246.
(48) Rohrer, M.; MacMillan, F.; Prisner, T. F.; Gardiner, A. T.; Möbius, K.; Lubitz, W. *J. Phys. Chem. B* **1998**, *102*, 4648−4657.
(49) Lubitz, W.; Feher, G. *Appl. Magn. Reson.* **1999**, *17*, 1−48.
(50) Paddock, M.; Abresch, E.; Isaacson, R.; Lubitz, W.; Okamura, M.; Feher, G. *Biophys. J.* **1999**, *76*, A141.
(51) Link, G.; Heinen, U.; Kothe, G. Unpublished results.

Table 2. Euler Angles Characterizing the Three-Dimensional Structure of the Light-Induced Radical Pair, $P_{865}^+Q_A^-$, in Reaction Centers of *Rb. Sphaeroides* R-26

orientation of the magnetic tensors[a]					*g*-tensor orientation of P_{865}^+[b]				
	global minimum value		systematic error[d]			angular values			
notation[c]	expt I	expt II	angular variation	confidence interval	notation[e]	orient. I	orient. II	orient. III	orient. IV
Φ_1	26°	28°	23°....30°	±4°	Φ_1^{dim}	189°	−**29**°	92°	105°
Θ_1	114°	113°	105°...121°	±8°	Θ_1^{dim}	38°	**23**°	112°	121°
Ψ_1	73°	79°	71°...80°	±5°	Ψ_1^{dim}	141°	**31**°	−70°	−127°
Θ_D	67°	65°	65°...69°	±3°					
Ψ_D	122°	123°	121°...124°	±2°					

[a] Evaluated in the present study from two-dimensional Q-band EPR experiments using the anisotropy of quantum beat oscillations. [b]Adapted from a single-crystal W-band EPR study of P_{865}^+.[29] A fourfold structural ambiguity (orientations I−IV) was eliminated by a combined analysis of the present Q-band and previous W-band EPR results. [c]The Euler angles Φ_1, Θ_1, Ψ_1, Θ_D, and Ψ_D relate the principal axis system of the respective magnetic tensor (*g*-tensor of P_{865}^+, dipolar tensor) and the magnetic reference system (*g*-tensor of Q_A^-). [d]The cited errors consider the uncertainties in the published *g*-tensor components. [e]The Euler angles Φ_1^{dim}, Θ_1^{dim}, and Ψ_1^{dim} relate the principal axis system of the *g*-tensor of P_{865}^+ and the molecular reference system (dimer system).[29]

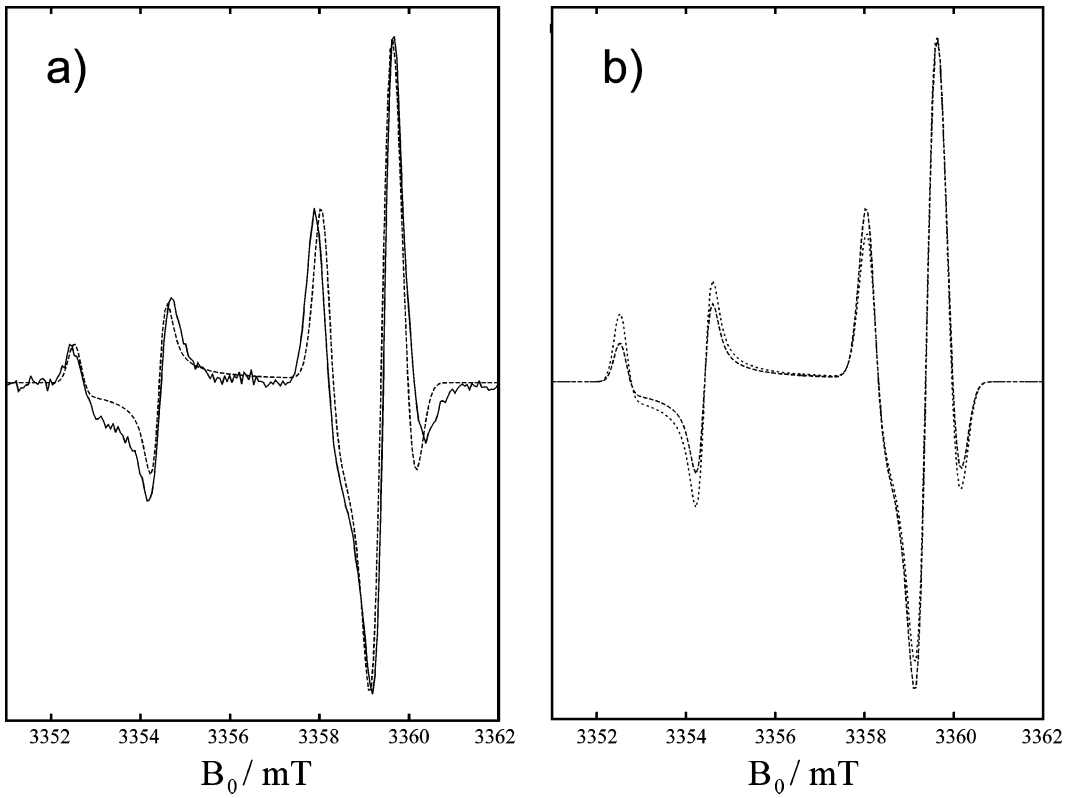

Figure 5. "Stationary" W-band EPR spectra of the light-induced radical pair $P_{865}^+Q_A^-$ in reaction centers of purple bacteria. Positive and negative signals indicate absorptive and emissive polarizations, respectively. Microwave frequency, $\omega/2\pi = 94.156$ GHz. Microwave field, $B_1 = 0.01$ mT. (a) Comparison of experimental and calculated line shapes. Full line: Experimental spectrum from deuterated and Zn-substituted reaction centers of *Rhodobacter sphaeroides* R-26 frozen in the dark. Temperature, $T = 90$ K. Dashed line: Calculated spectrum using the parameters given in Table 1. (b) Calculated line shapes for two different spatial orientations of Q_A^-. Dashed line: Conformation E (see Table 3, column 2). Dotted line: Conformation C (see Table 3, column 4).

microwave magnetic field of $B_1 = 0.06$ mT. A global fit of this experiment, involving 4900 data points, provided the parameter values (see Table 2)

$$\Phi_1 = 28° \pm 4°, \Theta_1 = 113° \pm 8°, \Psi_1 = 79° \pm 5°$$

$$\Theta_D = 65° \pm 3°, \Psi_D = 123° \pm 2°$$

Clearly, within the error limits, the same or magnetically equivalent magnetic tensor orientations were obtained. Thus, it appears that the underlying radical pair geometry, characterized by the five Euler angles Φ_1, Θ_1, Ψ_1, Θ_D, and Ψ_D, is basically correct.

In addition to the geometry parameters, the computer fit of the Q-band experiment also yields estimates of the statistical errors resulting from experimental noise. In general, however, the obtained statistical errors are well below 2° for all fitted angles.[52] Evidently, statistical errors do not provide useful estimates for the accuracy of the structure determination. Rather, systematic errors originating from the uncertainties in the fixed parameters should be employed in the evaluation of the method. In particular, variances in the published *g*-tensor components are expected to be a major source for systematic errors.[52]

(52) Heinen, U. Ph.D. Thesis, University of Freiburg, 2003.

First-order estimates of these errors can be obtained by repeating the geometry optimization procedure multiple times. In each run, one *g*-tensor component is stepped up or down according to its statistical error given in the literature. As a result one obtains a set of deviating structures clustered around the best-fit result. For each of the five Euler angles, characterizing the geometry of the radical pair, a nonlinear one-parameter confidence interval is then computed as a first-order estimate of the systematic error.[52] In Table 2, the angular variations and error intervals are listed together with the global minimum values from the two different Q-band experiments. One sees that the error intervals vary in a reasonable range between ±2° and ±8°.

To check the evaluated radical pair geometry, a W-band EPR study has been performed on the deuterated and Zn-substituted RCs of *Rb. sphaeroides* R-26. Spin-polarized W-band spectra of $P_{865}^{+}Q_A^{-}$ were measured using the transient nutation technique. As expected, no magneto-orientation effect was observed for the isolated RC proteins.[37] The W-band line shapes of $P_{865}^{+}Q_A^{-}$, recorded under different experimental conditions, always indicate an isotropic distribution of the radical pair with respect to the laboratory frame. A typical result is shown in Figure 5a. The experimental EPR spectrum (solid line), averaged in the time window 0.4−2.4 μs, refers to a microwave frequency of $\omega/2\pi = 94.156$ GHz, $B_1 = 0.01$ mT, and $T = 90$ K. Note the characteristic a/e/a/a/e/a/e polarization pattern which compares favorably with previous results obtained by Prisner et al.[21]

Because of the experimental parameters used, that is, a small microwave field and a large time window for signal averaging, a "stationary" EPR model[53] was applied in the analysis. The magnetic and structural parameters, used in the spectral simulation, were the same as those employed in the analysis of the two-dimensional Q-band EPR experiment (see Table 1). Hyperfine interactions in P_{865}^{+} and Q_A^{-} were considered by inhomogeneous Gaussian line widths. The dashed line in Figure 5a indicates the spectral simulation. Clearly, the agreement achieved is good.

Orientation of the *g*-Tensor of the Primary Donor. Analysis of the two-dimensional Q-band EPR experiment provides the orientation of the various magnetic tensors of $P_{865}^{+}Q_A^{-}$ with respect to a magnetic reference frame. To determine the mutual orientation of the cofactors P_{865}^{+} and Q_A^{-} in the radical pair, knowledge of the orientation of the *g*-tensors relative to the cofactors is required. This information exists for the quinone acceptor Q_A^{-}, in which the *g*-tensor axes are collinear with the molecular axes; i.e., the g^X component lies in the direction of the C−O carbonyl bond, while the g^Z axis is parallel to the normal of the quinone plane.[41] The situation is less clear for the primary donor P_{865}^{+}, where the spin density is delocalized over two closely positioned bacteriochlorophyll molecules (see Figure 6).[5,46] In fact, a large tilt angle was found between the g^Z axis and the average bacteriochlorophyll normal using single-crystal W-band EPR.[29] However, since the sign of the off-diagonal elements of the *g*-tensor cannot be determined in these experiments, a fourfold structural ambiguity remains.

To describe the *g*-tensor orientation of P_{865}^{+}, a molecular reference system was introduced which reflects the local symmetry of the primary donor.[29] The Z^{dim} axis is the average normal of the two bacteriochlorophylls each containing a Mg(II) ion in the center; the X^{dim} axis is the projection of the Mg−Mg direction onto the average bacteriochlorophyll plane. The Y^{dim} axis then describes the approximate local C_2 axis of the dimer, collinear with the membrane normal. In this reference system, the orientation of the *g*-tensor of P_{865}^{+} was described by four sets of Euler angles, denoted by orientation I, II, III, and IV (see Table 2, columns 6−10).[29]

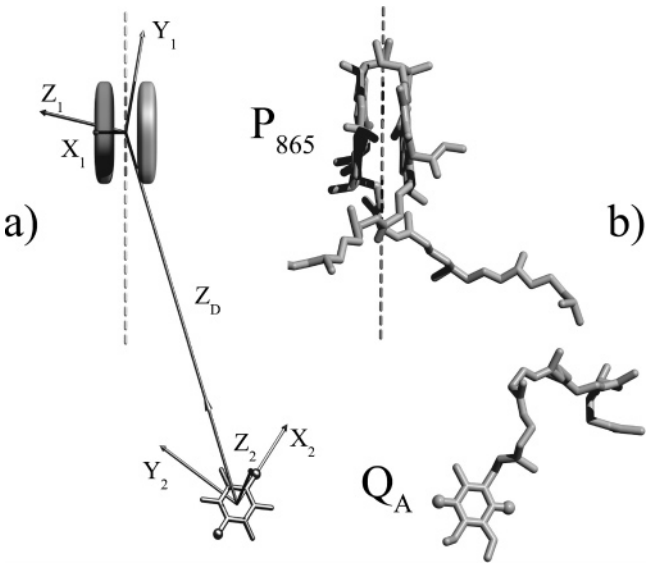

Figure 6. (a) Three-dimensional structure of the radical pair $P_{865}^{+}Q_A^{-}$ in reaction centers of purple bacteria determined by Q-band quantum beat oscillations in combination with single-crystal W-band EPR[29] (see Table 2). The shaded disks represent the two bacteriochlorophyll molecules of the primary donor P_{865}. The dashed line indicates the approximate local C_2 axis of the bacteriochlorophyll dimer, collinear with the membrane normal. $\mathbf{X}_1$, $\mathbf{Y}_1$, $\mathbf{Z}_1$ = principal axis system of the *g*-tensor of P_{865}^{+}. $\mathbf{X}_2$, $\mathbf{Y}_2$, $\mathbf{Z}_2$ = principal axis system of the *g*-tensor of the reduced secondary acceptor Q_A^{-}. $\mathbf{Z}_D$ = symmetry axis of the dipolar tensor. (b) Cofactor arrangement of the primary donor P_{865} and of the secondary acceptor Q_A as determined by X-ray crystallography.[4] The dashed line indicates the approximate local C_2 axis of the bacteriochlorophyll dimer.

This structural ambiguity can be eliminated by a critical evaluation of the radical pair structures calculated from the Q-band geometry and the four possible *g*-tensor orientations. The crucial parameter is the position of quinone A in the photosynthetic membrane. For *g*-tensor orientation II,

$$\Phi_1^{\mathrm{dim}} = -29°,\ \Theta_1^{\mathrm{dim}} = 23°,\ \Psi_1^{\mathrm{dim}} = 31°$$

Q_A^{-} is shifted by 2.5 Å from the position determined by X-ray crystallography. This shift appears to be insignificant in view of the uncertainty of the quinone position of ±4 Å,[52] calculated from the systematic errors of the Q-band study (see Table 2, columns 4 and 5).

On the other hand, use of *g*-tensor orientation I leads to a Q_A^{-} shift of 7 Å, which is well beyond the error limits. We believe that such a large shift is very unlikely to occur in the Q_A binding pocket of the RC protein. Consequently, *g*-tensor orientation I is eliminated. Similarly, the *g*-tensor orientations III and IV can be ignored since they lead to Q_A^{-} positions which are incompatible with the X-ray structure. We therefore conclude that *g*-tensor orientation II is correct. This conclusion confirms the previous assignment in a W-band EPR study of $P_{865}^{+}Q_A^{-}$.[21]

(53) Stehlik, D.; Bock, C. H.; Petersen, J. *J. Phys. Chem.* **1989**, *93*, 1612−1619.

Table 3. Comparison of the EPR Geometry of the Radical Pair, $P_{865}^+Q_A^-$, in Reaction Centers of *Rb. sphaeroides* with X-ray Diffraction Results

	EPR geometry[a]		X-ray diffraction results[b]	
notation[c]	angular value[d]	error[e]	angular value[f]	error[g]
Φ_2	**104°**	±5°	**164°**	**164°...179°**
Θ_2	113°	±8°	120°	99°...122°
Ψ_2	153°	±4°	161°	143°...163°
Θ_D'	65°	±8°	69°	68°...69°
Ψ_D'	106°	±7°	106°	99°...106°

[a] Evaluated in the present study using quantum beat oscillations observed in a two-dimensional Q-band EPR experiment. [b]Adapted from X-ray structures of the reaction center protein.[2−4,23] The angular values are based on *g*-tensor orientation II.[29] [c]The Euler angles specify the orientation (Φ_2, Θ_2, Ψ_2) and position (Θ_D', Ψ_D') of quinone A relative to the *g*-tensor system of P_{865}^+. [d]Average values from Q-band experiment I and II. [e]The cited errors are systematic errors, which consider the uncertainties in the published *g*-tensor components. [f]Representative X-ray diffraction result.[4] [g]Angular variation in five different X-ray structures of the same RC protein.[2−4,23]

Structure of the Charge Separated State. To determine the cofactor arrangement of $P_{865}^+Q_A^-$ in the photosynthetic membrane, knowledge of the orientation of one *g*-tensor in an external reference system is required. As noted above, this information exists for the primary donor P_{865}^+ where the *g*-tensor was determined by single-crystal W-band EPR.[29] Thus, using *g*-tensor orientation II, we obtain the three-dimensional structure of $P_{865}^+Q_A^-$ in the photosynthetic membrane, as shown in Figure 6a (left side). The structure describes the orientation of the *g*-tensor of P_{865}^+ as well as the position and orientation of the reduced acceptor, Q_A^-, a few tens of nanoseconds after light-induced charge separation. The new structural information is based on the analysis of quantum beat oscillations in combination with single-crystal high-field EPR.

Figure 6b (right side) shows the cofactor arrangement of P_{865} and Q_A as determined by X-ray crystallography.[4] Comparison with Figure 6a reveals that the position of the quinone in both structures is very similar. In fact, a minor shift of Q_A^- of 2.5 Å relative to the position of Q_A in the X-ray structure can be explained by the systematic errors of the EPR technique (see Table 2, column 5).[52] However, while the position of the quinone is indistinguishable between the EPR and X-ray structure, its orientation looks remarkably different. Figure 6 reveals that the head group of Q_A^- has undergone a 60° rotation in the ring plane relative to its orientation in the X-ray structure. Even with a cautious interpretation of the systematic errors of the EPR technique, such a rotation cannot be reconciled with the X-ray structure.

In Table 3 we present a detailed comparison of the EPR geometry of $P_{865}^+Q_A^-$ with the X-ray structure of the cofactors. For convenience, the *g*-tensor of P_{865}^+ is chosen as the molecular reference system. The Euler angles in column 1 specify the orientation (Φ_2, Θ_2, Ψ_2) and position (Θ_D', Ψ_D') of the quinone relative to the *g*-tensor system of P_{865}^+ (see Figure 6a). Column 2 summarizes the EPR geometry of $P_{865}^+Q_A^-$, obtained by computer analysis of the two-dimensional Q-band EPR experiments. The cited errors in column 3 are systematic errors, which consider the uncertainties in the published *g*-tensor components. Column 4 lists the cofactor geometry from a representative X-ray diffraction study.[4] The angular values are based on *g*-tensor orientation II.[29] Column 5 indicates the variation of the angular values in five different X-ray structures of the same RC protein.[2−4,23] This may serve as a crystal structure counterpart to the systematic errors estimated for the EPR technique. Interestingly, high-time resolution EPR provides the orientation of the quinone (Φ_2, Θ_2, Ψ_2) with a higher precision than X-ray diffraction of RC single crystals. Yet, the opposite is true for the position of the quinone (Θ_D',Ψ_D') where X-ray crystallography yields more precise results.

Inspection of Table 3 reveals that four out of the five listed Euler angles agree within the error limits. Only the angle Φ_2 deviates markedly between the two geometries. It is this angle which expresses the 60° rotation of Q_A^- in the ring plane relative to its orientation in the X-ray structure. Thus, analysis of quantum beat oscillations observed in a two-dimensional Q-band EPR experiment provides clear evidence for two structurally distinct states of the secondary acceptor, Q_A, in the RCs of purple bacteria.

Discussion

Assignment of the Two Conformational States of Q_A. The geometry of the charge separated state, $P_{865}^+Q_A^-$, in the RCs of purple bacteria has been determined by high-time resolution transient EPR, performed at Q-band frequency. Structural information was extracted from quantum beat oscillations observed at early times after laser excitation. Comparison with crystallographic data reveals that the position of Q_A^- is essentially the same as that in the X-ray structure. However, the orientation of Q_A^- is found to be remarkably different. In fact, the head group of Q_A^- has undergone a 60° rotation in the ring plane relative to its orientation in the crystal structure. This structural change suggests that Q_A possibly plays a more active role in the electron transfer from Q_A^- to Q_B than previously anticipated.

Figure 7 depicts the spatial arrangement of the two conformational states of Q_A in the photosynthetic membrane together with other cofactors of the electron-transfer chain. One sees that the two Q_A conformations differ from each other in the spatial orientation of the carbonyl bonds, which is relevant to the rate of the electron transfer. Interestingly, in the EPR conformation (conformation E) (see Figure 7b), one carbonyl bond is oriented toward a methylester group of the primary acceptor, Φ_A, whereas, in the crystal conformation (conformation C) (see Figure 7a), another carbonyl bond points directly to a carbonyl bond of the tertiary acceptor, Q_B. This suggests that the light-induced electron transfer in the RCs of purple bacteria proceeds via two different states of Q_A, each optimized for another electron-transfer step. It appears that conformation E is associated with the electron transfer from Φ_A^- to Q_A and that conformation C is involved in the electron transfer from Q_A^- to Q_B.

To check this intriguing notion, we first examine conformation E, derived from the EPR structure of $P_{865}^+Q_A^-$ (see Figure 7b). Notably, this structure describes a trapped state in which electron transfer between Q_A^- and Q_B cannot occur. It is obtained at 70 K a few tens of nanoseconds after light-induced charge separation. Since large-scale motions of Q_A^- are unlikely to occur under these conditions, we identify conformation E with the arrangement of Q_A prior to the electron transfer from Φ_A^-. In other words, conformation E represents the spatial arrangement of the neutral Q_A in the dark adapted RC protein.

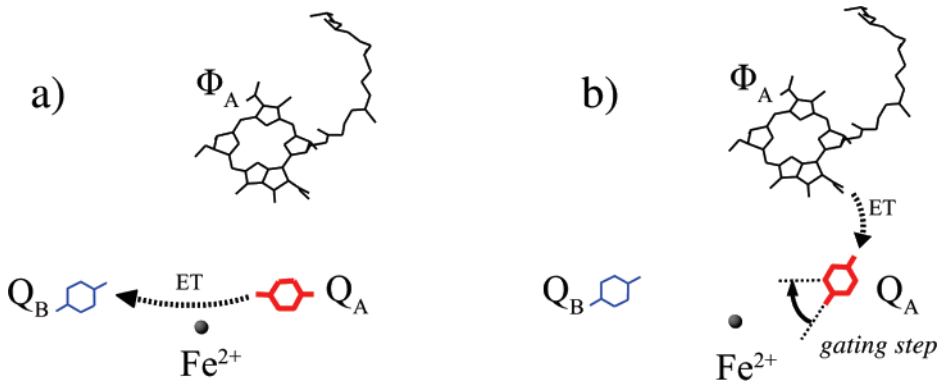

Figure 7. Spatial arrangement of the two conformational states of the secondary acceptor Q_A together with other cofactors of the electron-transfer chain in reaction centers of *Rhodobacter sphaeroides*. (a) The crystal conformation (conformation C) is adapted from a high-resolution X-ray structure of the reaction center protein.[4] (b) The EPR conformation (conformation E) is determined in the present study using quantum beat oscillations. Φ_A = bacteriopheophytin acceptor, Q_B = tertiary acceptor. The dotted arrows indicate two electron transfer (ET) steps. The full arrow denotes the gating step preceding the electron transfer from Q_A^- to Q_B.

Let us now examine conformation C, determined by X-ray crystallography (see Figure 7a). Comparison reveals that the quinone is rotated by 60° relative to the orientation of conformation E, the neutral Q_A in the dark adapted RC protein (see Figure 7b). How do we explain this structural change? Is it functionally important? One possible explanation is specific radiation chemistry, observed in protein crystallography performed as a function of the X-ray dose.[28] It was noticed that radiation-induced photoelectrons are trapped at specific susceptible groups, which then undergo structural and chemical alterations, including breakage of disulfide bonds and decarboxylation.[28]

Recently, specific radiation chemistry was also observed in two RC proteins.[54,55] X-ray absorption spectra of photosystem II revealed that the structure of the Mn_4Ca complex changes from a high-valent $Mn_2(III_2,IV_2)$ cluster to that of Mn(II) in aqueous solution.[55] This drastic structural change occurs at an X-ray dose that is more than 1 order of magnitude lower than the dose commonly considered safe for protein crystallography. Moreover, a test study of radiation damage in single crystals of Fe-removed, Zn-substituted *Rb. sphaeroides* RCs demonstrates that low doses of irradiation lead to a loss of photosynthetic activity.[56] In this case it is very likely that the crystal structure displays the spatial arrangement of the reduced quinone Q_A^- which differs from that of the neutral species, Q_A, by a 60° rotation of the headgroup.

Support for the assignment of conformation C comes from a single-crystal Q-band EPR study of the *g*-tensor of Q_A^- in the RC protein.[43] It was found that the spatial orientation of the semiquinone Q_A^-, as determined by the *g*-tensor axes, deviates only a few degrees from the orientation of quinone A in the X-ray structure.[43] These previous EPR results in combination with the distinct spatial orientation of conformation E we observe suggest that specific radiation chemistry at the Q_A site occurred in the crystal structure. Consequently, we identify conformation C with the spatial arrangement of the reduced quinone Q_A^-.

Gating Process of the Electron Transfer from Q_A^- to Q_B. The rate of electron transfer from Q_A^- to Q_B, k_{AB}, was measured in RCs of *Rb. sphaeroides* by replacing the native ubiquinone-10 in the Q_A binding site with quinones having different redox potentials.[22] The results showed that k_{AB} does not change as the redox free energy for electron transfer is varied. It was therefore concluded that the Q_A^- to Q_B electron transfer is conformationally gated, i.e., that the rate-limiting step is a conformational change required before electron transfer.[22] This change was proposed to be a movement of Q_B as observed in an X-ray study of the RC protein, frozen under illumination and in the dark.[23] However, recent FTIR studies of RCs of *Rb. sphaeroides* suggest that this movement of Q_B is not related to the $Q_A^- \rightarrow Q_B$ electron transfer.[25]

Having identified two different conformations of Q_A^-, we are able to propose an alternative gating process. Our model involves four consecutive steps,

$$P_{865}Q_A(E)Q_B \xrightarrow{h\nu} P_{865}^+Q_A^-(E)Q_B \xrightarrow{k_C} P_{865}^+Q_A^-(C)Q_B \xrightarrow{k_{ET}} P_{865}^+Q_A(C)Q_B^- \xrightarrow{k_R} P_{865}^+Q_A(E)Q_B^- \quad (4)$$

as schematically depicted in Figure 7. We assume that the conformations E and C are functionally relevant states which control the electron transfer from Q_A^- to Q_B. In conformation E, Q_A^- is in an inactive state and electron transfer is impaired. In conformation C, Q_A^- is in the active configuration and electron transfer can proceed. Our time-resolved EPR studies indicate that, in the dark, Q_A is predominantly in the E state.

Light excitation results in the formation of $P_{865}^+Q_A^-$ (E) where Q_A^- is in the inactive conformation (see Figure 7b). Conversion to the active conformation, $Q_A^-(E) \rightarrow Q_A^-(C)$, occurs with the conformational gating rate k_C. The gating step involves a 60° rotation of the headgroup of the quinone in the Q_A binding pocket (see Figure 7b). Once Q_A^- is in the active configuration, the electron transfer $Q_A^-(C)Q_B \rightarrow Q_A(C)Q_B^-$ can occur with a rate k_{ET} (see Figure 7a). After the electron transfer, Q_A relaxes back to conformation E, $Q_A(C) \rightarrow Q_A(E)$, characteristic of the neutral quinone in the dark adapted protein. The rate of this process is k_R.

Thus, we propose that the conformational gate for the $Q_A^- \rightarrow Q_B$ electron transfer is a movement of Q_A^- in its binding pocket

(54) Baxter, R. H. G.; Seagle, B.-L.; Ponomarenko, N.; Norris, J. R. *J. Am. Chem. Soc.* **2004**, *126*, 16728−16729.
(55) Yano, J.; Kern, J.; Irrgang, K.-D.; Latiner, M. J.; Bergmann, U.; Glatzel, P.; Pushkar, Y.; Biesiadka, J.; Loll, B.; Sauer, K.; Messinger, J.; Zouni, A.; Yachandra, V. K. *Proc. Natl. Acad. Sci. U.S.A.* **2005**, *107*, 12047−12052.
(56) Poluektov, O. G.; Utschig, L. M. Unpublished results.

upon light-induced reduction (see Figure 7b). We expect that this movement is associated with a change in the hydrogen bonding interactions of Q_A^- to nearby amino acid residues and/or protein backbone protons. Support for this notion comes from a previous FTIR study indicating that light-induced Q_A reduction causes a large change in the bonding interactions between the quinone carbonyls and the protein.[26]

Low-temperature time-resolved high-field ENDOR of $P_{865}^+Q_A^-$ revealed that the positions of the ENDOR lines of Q_A^- shift with an increase in time after the laser flash, which initiates formation of $P_{865}^+Q_A^-$.[57] Are these shifts related to the proposed gating step for the $Q_A^- \rightarrow Q_B$ electron transfer? We think that this is not the case simply because at low temperature the electron transfer does not occur any more. Rather, we believe that the time-dependent shifts are direct spectroscopic evidence of reorganization of the protein environment accommodating the negative charge at site Q_A.

The gating model requires that the observed overall rate for the electron transfer is equal to the gating rate, i.e., $k_{AB} = k_C$. This allows for direct measurement of the kinetics of the gating process, using time-resolved optical spectroscopy.[22,58] The observed time constant of $1/k_C \simeq 100$ μs (296 K)[22,58] is compatible with the proposed gating step, involving a 60° rotation of Q_A^- in its binding pocket. Measurement of the temperature dependence of k_{AB} provides a small activation energy of $E_a = 115$ meV (273 K < T < 300 K),[58] suggesting that there is ample space for the Q_A^- reorientation in the RC protein.[59]

The proposed model accounts for a striking observation by Kleinfeld et al.[60] These authors reported that electron transfer from Q_A^- to Q_B proceeds in RCs cooled to cryogenic temperature under illumination but does not proceed in RCs cooled in the dark.[60] RCs frozen in the dark are trapped in the inactive conformation E. At low temperature, there is insufficient thermal energy for conformational interconversion and thus electron transfer is impaired. RCs cooled under illumination are trapped in the active state (conformation C) which allows for electron transfer even at cryogenic temperature.

The model also accounts for another surprising observation made on RCs containing only quinone A.[60] When these RCs were cooled in the dark, the charge recombination time of the process $P_{865}^+Q_A^- \rightarrow P_{865}Q_A$ was $\tau_{AP}^{dark} \approx 25$ ms (77 K).[60] When the same RCs were cooled under illumination, the charge recombination time changed to $\tau_{AP}^{light} \approx 120$ ms (77 K).[59] One can easily rationalize these findings in terms of two distinct Q_A^- conformations as depicted in Figure 7. RCs frozen in the dark are trapped in conformation E, while RCs cooled under illumination are trapped in conformation C.

Light-Induced Movement of Q_A^-. We have proposed a new gating mechanism for the $Q_A^- \rightarrow Q_B$ electron-transfer kinetics in RCs of purple bacteria. The suggested gating step involves a rotation of the headgroup of Q_A^- in its binding pocket as a response to light-induced reduction (see Figure 7). The model is based on the results of the present EPR study, which provides clear evidence for two structurally distinct Q_A^- conformations.

Previously, Abresch et al. searched for light-induced structural changes of Q_A using X-ray crystallography.[61] The authors studied single crystals of RCs from *Rb. sphaeroides* which were frozen under illumination to trap the $P_{865}^+Q_A^-$ state. A 98% complete 3 Å resolution data set was collected at 70 K. The model of the data showed no changes within the error between the superimposed coordinate sets of the "light" structure and the "dark" structure obtained at 2.2 Å.[61] In both structures the position and orientation of Q_A was practically identical. How can we rationalize these findings in view of the present EPR results? A plausible explanation is specific radiation chemistry at the quinone sites of the RC protein.[28,54−56] Then, due to radiation-induced reduction, even dark adapted crystals display the spatial arrangement of the semiquinone Q_A^-.

Possible light-induced structural changes of Q_A^- were also explored by time-resolved EPR of the spin-correlated radical pair $P_{865}^+Q_A^-$ in RCs of *Rb. sphaeroides*.[62] Zech et al. reported a difference in the lifetime of $P_{865}^+Q_A^-$ between RCs frozen in the light, $\tau^{light} \approx 101$ ms (80 K), and in the dark, $\tau^{dark} \approx 27$ ms (80 K).[62] These findings compare favorably with the results by Kleinfeld et al. who determined similar values for the charge recombination time of the radical pair using time-resolved optical spectroscopy.[60] The difference between τ^{light} and τ^{dark} can, in principle, be explained by a change in the distance and/or relative orientation of P_{865}^+ and Q_A^-.

From the out-of-phase echo modulation pattern, observed in a pulsed EPR experiment, it was deduced that the distance between P_{865}^+ and Q_A^- is the same in dark frozen samples and in those frozen under illumination.[62] This is in agreement with the present EPR results, indicating that the position of Q_A^- does not vary between the EPR and the X-ray structure (see Figure 6). To check whether there is a light-induced Q_A^- reorientation, Zech et al. studied the "stationary" Q-band EPR spectra of $P_{865}^+Q_A^-$ in deuterated RCs of *Rb. sphaeroides*.[62] Surprisingly, no major spectral changes were observed for samples cooled under illumination as compared to those frozen in the dark.[62] How can we reconcile this observation with the proposed light-induced Q_A^- reorientation?

To clarify this point, we have calculated the spin-polarized W-band spectrum of $P_{865}^+Q_A^-$ for the two Q_A^- conformations using the "stationary" EPR model of spin-correlated radical pairs.[53] In this model, the nonsecular terms of the electron spin−spin interactions are omitted. The result is shown in Figure 5b. The dashed line refers to conformation E, while the dotted line denotes conformation C. Evidently, the two Q_A^- orientations cannot be distinguished by the "stationary" W-band EPR spectra of $P_{865}^+Q_A^-$. This is similarly true for the corresponding Q-band line shapes. This coincidence of the spectra may well explain why the light-induced Q_A^- reorientation has not yet been detected.

Recently, an elegant analytical method was presented to extract the geometry of weakly coupled radical pairs from their "stationary" polarization patterns.[63,64] This treatment also shows

(57) Poluektov, O. G.; Utschig, L. M.; Dubinskii, A.; Thurnauer, M. C. *J. Am. Chem. Soc.* **2005**, *127*, 4049−4059.
(58) Li, J.; Gilroy, D.; Tiede, D. M.; Gunner, M. R. *Biochemistry* **1998**, *37*, 2818−2829.
(59) Allen, J.; Feher, G.; Yeates, T.; Komiya, H.; Rees, D. *Proc. Natl. Acad. Sci. U.S.A.* **1988**, *85*, 8487−8491.
(60) Kleinfeld, D.; Okamura, M. Y.; Feher, G. *Biochemistry* **1984**, *23*, 5780−5786.
(61) Abresch, E. C.; Yeh, A. P.; Soltis, S. M.; Rees, D. C.; Axelrod, H. L.; Okamura, Y. M.; Feher, G. *Biophys. J.* **1999**, *76*, A141.
(62) Zech, S. G.; Bittl, R.; Gardiner, A. T.; Lubitz, W. *Appl. Magn. Reson.* **1997**, *13*, 517−529.
(63) Kandrashkin, Y.; van der Est, A. *Spectrochim. Acta* **2001**, *A57*, 1697−1709.

the restrictions placed on the information obtainable from such spectra. Most importantly, only four out of the five Euler angles, characterizing the geometry of a radical pair, can be extracted. Moreover, a unique set of angles is only obtained if the absolute amplitude of the spectrum is known.[63,64] These restrictions can be overcome by studying the spin dynamics of the radical pair at early times after pulsed laser excitation. In fact, analysis of quantum beat oscillations observed in a two-dimensional Q-band EPR experiment provides clear evidence for two different conformations of the secondary acceptor, Q_A^-, in the RCs of purple bacteria.

Just before finishing the present article, a very recent publication by Savitsky et al. came to our notice.[65] The authors used orientation-resolved pulsed electron dipolar high-field EPR spectroscopy to determine the cofactor arrangement of $P_{865}^+Q_A^-$. Similar to the quantum beat method,[27] this technique can also provide all five Euler angles of the radical pair geometry. The structure obtained for $P_{865}^+Q_A^-$[65] still differs somewhat from that evaluated in the present study. The reason for this deviation is not yet clear.

Conclusions

We have evaluated the three-dimensional structure of the secondary radical pair $P_{865}^+Q_A^-$ in RCs of purple bacteria using quantum beat oscillations[27] in combination with high-field single-crystal EPR.[29] Thus, we have obtained the cofactor arrangement of $P_{865}^+Q_A^-$ on a nanosecond time scale after light-induced charge separation. The structure describes the position and orientation of the reduced quinone acceptor Q_A^- in the photosynthetic membrane, which we suggest reflects the neutral Q_A in the dark adapted protein.

Comparison with crystallographic data reveals that the position of the quinone in the EPR and X-ray structures is very similar. However, the head group of Q_A^- is rotated by 60° relative to its orientation in the crystal structure. Even with a cautious interpretation of the systematic errors of the EPR technique such a rotation cannot be reconciled with the crystallographic data. Thus, study of quantum beat oscillations, observed in a two-dimensional Q-band experiment, provides clear evidence for two structurally distinct states of the primary quinone acceptor, Q_A, in the RCs of purple bacteria.

Analysis suggests that the two different Q_A conformations are functionally relevant states which control the electron-transfer kinetics from Q_A^- to the secondary quinone acceptor Q_B. It appears that the rate-limiting step of this reaction is a light-induced reorientation of Q_A^- in its binding pocket. Thus, we have demonstrated that analysis of quantum oscillations can help in understanding the function of the primary quinone acceptor in the electron-transfer chain of photosynthetic bacteria.

Although our study was restricted to RC proteins of purple bacteria, quantum oscillations of spin-correlated radical pairs are a common feature of systems that undergo efficient light-induced charge separation. Apparently, these shared characteristics of natural and artificial systems, as revealed through high-time resolution EPR,[27,66,67] reflect underlying fundamental structural and energetic requirements for efficient charge separation. Therefore, high-time resolution EPR continues to yield new insights into photochemical energy conversion in natural and artificial photosynthetic systems.

Acknowledgment. The authors would like to thank M. C. Thurnauer for initiating this study and for stimulating discussions in the course of the work. Research in the Freiburg laboratory was supported by the DFG priority program "High-field EPR in Biology, Chemistry and Physics" (SPP 1051) and by a grant from the Ministry of Science, Research and the Arts of Baden-Württemberg (24-7532.23-1-11/1). Work at Argonne was supported by the U.S. Department of Energy, Office of Basic Energy Sciences, Division of Chemical Sciences, Geosciences and Biosciences under Contract W-31-109-Eng-38.

JA075065H

(64) Dubinskii, A. A.; Perekhodtsev, G. D.; Poluektov, O. G.; Rajh, T.; Thurnauer, M. C. *J. Phys. Chem. B* **2002**, *106*, 938−944.
(65) Savitsky, A.; Dubinskii, A. A.; Flores, M.; Lubitz, W.; Möbius, K. *J. Phys. Chem. B* **2007**, *111*, 6245−6262.
(66) Kiefer, A. M.; Kast, S. M.; Wasielewski, M. R.; Laukenmann, K.; Kothe, G. *J. Am. Chem. Soc.* **1999**, *121*, 188−198.
(67) Kothe, G.; Norris, J. R.; Poluektov, O. G.; Thurnauer, M. C. In *Biophysical Techniques in Photosynthesis II*; Aartsma, T. J., Matysik, J., Eds.; Springer: Dordrecht, 2007; pp 305−323.